

Performance Comparison of Backstepping-Based Adaptive Controllers for Marine Surface Vessels

Mikkel Eske Nørgaard Sørensen* Elias S. Bjørne* Morten Breivik*

Abstract—This paper deals with the design and evaluation of three controllers based on backstepping and different adaptive control schemes, which are applied to the motion control of a nonlinear 3 degrees-of-freedom model of a marine surface vessel. The goal is to make a comparative analysis of the controllers in order to find out which one has the best performance. The considered controllers are: Adaptive backstepping, backstepping with composite concurrent learning and backstepping with cascaded concurrent learning. Numerical simulations are performed for target tracking along an elliptic path, with uncertain vessel model parameters. Motion control performance is evaluated by performance metrics such as IAE and a novel metric named IAEW-WT which combines control accuracy, energy use and actuator wear and tear in one single metric.

Index Terms—Marine surface vessel, Nonlinear motion control, Adaptive backstepping, Concurrent learning, Composite adaptation, Cascaded adaptation, Performance metrics

I. INTRODUCTION

Automated motion control of marine surface vessels has been a research topic since the early 20th century. In recent years, the research has expanded from control of manned vessels to also include unmanned vessels. Challenges include uncertain nonlinear hydrodynamics and external disturbances, since the ocean is an unreliable environment with nonlinearities and unpredictable events. The hydrodynamic forces are often modelled with hydrodynamical coefficients. However, it is typically only a few of these coefficients that can be found. External disturbances such as waves, wind and current are also difficult to measure. Hence, it is important to develop adaptive and robust control algorithms, which can deal with these model uncertainties and external disturbances in a precise and energy-efficient manner.

An overview of some of the recent developments of state-of-the-art adaptive control methods are given in [1], [2], [3] and [4]. In [5], a comparative analysis of various adaptive controllers is made in order to investigate which one has the best control performance by using performance metrics.

An adaptation method which has received attention in recent years is concurrent learning (CL). In [6], it is shown that for an adaptive controller which uses both recorded and instantaneous data concurrently for adaptation, a verifiable condition on linear independence of the recorded data is sufficient to guarantee exponential convergence of the tracking

*M. E. N. Sørensen, E. S. Bjørne and M. Breivik are with the Department of Engineering Cybernetics, Norwegian University of Science and Technology (NTNU), NO-7491 Trondheim, Norway. (Email: mikkelsorensen@itk.ntnu.no, eliasbjorne@gmail.com, morten.breivik@ieee.org)

Additionally, M. E. N. Sørensen and M. Breivik are associated with the NTNU Centre for Autonomous Marine Operations and Systems.

and parameter errors. Concurrent learning is combined with a model reference adaptive control (MRAC) algorithm to improve the trajectory tracking performance of a quadrotor in [7]. The tracking performance is compared against a traditional MRAC algorithm and a standard PID controller using the root mean square error. In [8], a concurrent learning MRAC method is developed for handling linear uncertain dynamical systems, where the sign of the control signal and parameters of the control allocation matrix are unknown.

This paper is based on the work in [9]. Here, we suggest new adaptive control approaches by combining the concurrent learning concept from [6] with a traditional backstepping controller. The tracking performance is compared against the standard adaptive backstepping controller [10] as a benchmark controller. Simulation results are made using a fully actuated 3 degrees-of-freedom model of a marine surface vessel [11]. The results show that the adaptive controller based on concurrent learning achieves better and more energy-efficient tracking performance than the benchmark controller. However, the CL controllers require acceleration measurements which the benchmark controller does not.

The structure of this paper is as follows: A mathematical vessel model and assumptions are presented in Section II; Section III presents the design of the considered adaptive controllers for a vessel with model uncertainties; Section IV includes simulation results and performance evaluation; while Section V concludes the paper.

II. MARINE SURFACE VESSEL MODEL

The motion of a surface vessel can be represented by the pose vector $\eta = [x, y, \psi]^T \in \mathbb{R}^2 \times \mathbb{S}$ and the velocity vector $\nu = [u, v, r]^T \in \mathbb{R}^3$, where $\mathbb{S} \in [-\pi, \pi]$. Here, (x, y) represents the Cartesian position in the local reference frame, ψ is the yaw angle, (u, v) represents the body-fixed linear velocities and r is the yaw rate. The 3 degrees-of-freedom dynamics of a surface vessel can be stated as [12]:

$$\dot{\eta} = \mathbf{R}(\psi)\nu \quad (1)$$

$$M\dot{\nu} + C(\nu)\nu + D(\nu)\nu = \tau, \quad (2)$$

where

$$\mathbf{R}(\psi) = \begin{bmatrix} \cos(\psi) & -\sin(\psi) & 0 \\ \sin(\psi) & \cos(\psi) & 0 \\ 0 & 0 & 1 \end{bmatrix}, \quad (3)$$

is a rotation matrix $\mathbf{R} \in SO(3)$, and where M , $C(\nu)$, $D(\nu)$ and τ represent the inertia matrix, Coriolis and centripetal matrix, damping matrix and control input vector, respectively. The system matrices are assumed to satisfy

the properties $M = M^\top > 0$, $C(\boldsymbol{\nu}) = -C^\top(\boldsymbol{\nu})$ and $D(\boldsymbol{\nu}) > 0$.

However, there are uncertainties associated with these system matrices. This paper will base the relationship between the real and considered system matrices upon the assumption made in [13], where all the inertia coefficients and some of the hydrodynamic coefficients are assumed to be known, which changes (2) to

$$M\dot{\boldsymbol{\nu}} + C(\boldsymbol{\nu})\boldsymbol{\nu} - \mathbf{g}(\boldsymbol{\nu}) - \Phi(\boldsymbol{\nu})\boldsymbol{\varphi}^* = \boldsymbol{\tau}. \quad (4)$$

Here,

$$\mathbf{g}(\boldsymbol{\nu}) = [X_u u, Y_v v, N_v v]^\top, \quad (5)$$

is the known part of $D(\boldsymbol{\nu})\boldsymbol{\nu}$, while

$$\Phi(\boldsymbol{\nu}) \triangleq \begin{bmatrix} u^3 & |u|u & 0 & 0 & 0 & 0 & 0 & 0 & 0 & 0 & 0 & 0 \\ 0 & 0 & |v|v & |r|v & r & |v|r & |r|r & 0 & 0 & 0 & 0 & 0 \\ 0 & 0 & 0 & 0 & 0 & 0 & 0 & |v|v & |r|v & r & |v|r & |r|r \end{bmatrix}, \quad (6)$$

$$\boldsymbol{\varphi}^* \triangleq [X_{uuu}^*, X_{|u|u}^*, Y_{|v|v}^*, Y_{|r|v}^*, Y_r^*, Y_{|v|r}^*, Y_{|r|r}^*, N_{|v|v}^*, N_{|r|v}^*, N_r^*, N_{|v|r}^*, N_{|r|r}^*]^\top \quad (7)$$

are the regressor matrix and the vector of unknown parameters, respectively, such that

$$\mathbf{g}(\boldsymbol{\nu}) + \Phi(\boldsymbol{\nu})\boldsymbol{\varphi}^* = -D(\boldsymbol{\nu})\boldsymbol{\nu}. \quad (8)$$

Additionally, it is assumed that $\dot{\boldsymbol{\varphi}}^* = \mathbf{0}$, i.e., the uncertainties are constant or slowly varying relative to the vessel dynamics.

It is furthermore assumed that the pose vector $\boldsymbol{\eta}$ and velocity vector $\boldsymbol{\nu}$ can be measured. Finally, it is assumed that there are no magnitude or rate saturation constraints for the control input $\boldsymbol{\tau}$.

III. CONTROLLER DESIGN

The control objective is to make $\tilde{\boldsymbol{\eta}}(t) \triangleq \boldsymbol{\eta}(t) - \boldsymbol{\eta}_t(t) \rightarrow \mathbf{0}$ as $t \rightarrow \infty$, where $\boldsymbol{\eta}_t(t) = [x_t(t), y_t(t), \psi_t(t)]^\top \in \mathbb{R}^2 \times \mathbb{S}$ represents the pose associated with a target point, which is \mathcal{C}^2 and bounded. The motion of the target is typically defined by a human or generated by a guidance system.

In this section, we will start by designing a benchmark controller based on a standard adaptive backstepping controller, and subsequently extend and change it by incorporating the concurrent learning concept in two different ways.

The backstepping controller design is divided into two stages, including the definition of state variables and deriving the control laws through control Lyapunov functions (CLFs). The design is based on the backstepping method, which has been applied in e.g. [5] and [14].

For notational simplicity, the time t is omitted in the following.

A. Adaptive Backstepping Control

Start by defining the error variables \mathbf{z}_1 and \mathbf{z}_2 :

$$\mathbf{z}_1 \triangleq \mathbf{R}^\top(\psi)(\boldsymbol{\eta} - \boldsymbol{\eta}_t) \quad (9)$$

$$\mathbf{z}_2 \triangleq \boldsymbol{\nu} - \boldsymbol{\alpha}, \quad (10)$$

where $\boldsymbol{\alpha} \in \mathbb{R}^3$ is a so-called stabilising function, which can be interpreted as a desired velocity and which is to be designed later.

1) *Step 1:*

Choosing the positive definite CLF

$$V_1 \triangleq \frac{1}{2} \mathbf{z}_1^\top \mathbf{z}_1, \quad (11)$$

the derivative of V_1 with respect to time along the \mathbf{z}_1 -dynamics gives

$$\begin{aligned} \dot{V}_1 &= \mathbf{z}_1^\top \dot{\mathbf{z}}_1 \\ &= \mathbf{z}_1^\top (\mathbf{S}^\top(r) \mathbf{R}^\top(\psi)(\boldsymbol{\eta} - \boldsymbol{\eta}_t) + \mathbf{R}^\top(\psi)(\dot{\boldsymbol{\eta}} - \dot{\boldsymbol{\eta}}_t)) \\ &= \mathbf{z}_1^\top (\mathbf{S}^\top(r) \mathbf{z}_1 + \mathbf{R}^\top(\psi)(\dot{\boldsymbol{\eta}} - \dot{\boldsymbol{\eta}}_t)), \end{aligned} \quad (12)$$

where

$$\mathbf{S}(r) = \begin{bmatrix} 0 & -r & 0 \\ r & 0 & 0 \\ 0 & 0 & 0 \end{bmatrix} \quad (13)$$

is a skew-symmetric matrix satisfying $\mathbf{z}_1^\top \mathbf{S}^\top(r) \mathbf{z}_1 = 0$, which gives

$$\dot{V}_1 = \mathbf{z}_1^\top (\boldsymbol{\nu} - \mathbf{R}^\top(\psi) \dot{\boldsymbol{\eta}}_t). \quad (14)$$

Using (10), the CLF becomes

$$\begin{aligned} \dot{V}_1 &= \mathbf{z}_1^\top (\mathbf{z}_2 + \boldsymbol{\alpha} - \mathbf{R}^\top(\psi) \dot{\boldsymbol{\eta}}_t) \\ &= \mathbf{z}_1^\top \mathbf{z}_2 + \mathbf{z}_1^\top (\boldsymbol{\alpha} - \mathbf{R}^\top(\psi) \dot{\boldsymbol{\eta}}_t), \end{aligned} \quad (15)$$

where the stabilising function can be chosen as

$$\boldsymbol{\alpha} = \mathbf{R}^\top(\psi) \dot{\boldsymbol{\eta}}_t - \mathbf{K}_1 \mathbf{z}_1 \quad (16)$$

with $\mathbf{K}_1 > 0$, which results in

$$\dot{V}_1 = -\mathbf{z}_1^\top \mathbf{K}_1 \mathbf{z}_1 + \mathbf{z}_1^\top \mathbf{z}_2, \quad (17)$$

and the \mathbf{z}_1 -dynamics becomes

$$\dot{\mathbf{z}}_1 = \mathbf{S}^\top(r) \mathbf{z}_1 - \mathbf{K}_1 \mathbf{z}_1 + \mathbf{z}_2. \quad (18)$$

2) *Step 2:*

The \mathbf{z}_2 -dynamics can be written as

$$\begin{aligned} \mathbf{M} \dot{\mathbf{z}}_2 &= \mathbf{M}(\dot{\boldsymbol{\nu}} - \dot{\boldsymbol{\alpha}}) \\ &= \boldsymbol{\tau} - \mathbf{C}(\boldsymbol{\nu})\boldsymbol{\nu} + \mathbf{g}(\boldsymbol{\nu}) + \Phi(\boldsymbol{\nu})\boldsymbol{\varphi}^* - \mathbf{M}\dot{\boldsymbol{\alpha}}, \end{aligned} \quad (19)$$

where the time derivative of (16) becomes

$$\dot{\boldsymbol{\alpha}} = \mathbf{R}^\top(\psi) \ddot{\boldsymbol{\eta}}_t + \mathbf{S}(r)^\top \mathbf{R}^\top(\psi) \dot{\boldsymbol{\eta}}_t - \mathbf{K}_1 \dot{\mathbf{z}}_1. \quad (20)$$

The CLF for both \mathbf{z}_1 and \mathbf{z}_2 is then defined as

$$V_2 \triangleq \frac{1}{2} \mathbf{z}_2^\top \mathbf{M} \mathbf{z}_2 + V_1. \quad (21)$$

Simplifying $\mathbf{C}(\boldsymbol{\nu}) = \mathbf{C}$, $\mathbf{g}(\boldsymbol{\nu}) = \mathbf{g}$, $\Phi(\boldsymbol{\nu}) = \Phi$, $\mathbf{R}(\boldsymbol{\nu}) = \mathbf{R}$ and $\mathbf{S}(r) = \mathbf{S}$ for notational brevity, the derivative of (21) becomes

$$\begin{aligned}\dot{V}_2 &= \mathbf{z}_2^\top \mathbf{M} \dot{\mathbf{z}}_2 + \dot{V}_1 \\ &= \mathbf{z}_2^\top (\boldsymbol{\tau} - \mathbf{C}\boldsymbol{\nu} + \mathbf{g} + \Phi \boldsymbol{\varphi}^* - \mathbf{M}\dot{\boldsymbol{\alpha}}) \\ &\quad - \mathbf{z}_1^\top \mathbf{K}_1 \mathbf{z}_1 + \mathbf{z}_1^\top \mathbf{z}_2.\end{aligned}\quad (22)$$

The control input can be chosen as

$$\boldsymbol{\tau} = \mathbf{M}\dot{\boldsymbol{\alpha}} + \mathbf{C}\boldsymbol{\nu} - \mathbf{g} - \Phi \boldsymbol{\varphi}^* - \mathbf{z}_1 - \mathbf{K}_2 \mathbf{z}_2, \quad (23)$$

where $\mathbf{K}_2 > 0$, which results in

$$\dot{V}_2 = -\mathbf{z}_1^\top \mathbf{K}_1 \mathbf{z}_1 - \mathbf{z}_2^\top \mathbf{K}_2 \mathbf{z}_2 < 0, \quad (24)$$

which makes the origin of the \mathbf{z} -dynamics

$$\dot{\mathbf{z}}_1 = \mathbf{S}^\top \mathbf{z}_1 - \mathbf{K}_1 \mathbf{z}_1 + \mathbf{z}_2 \quad (25)$$

$$\dot{\mathbf{z}}_2 = -\mathbf{M}^{-1}(\mathbf{z}_1 + \mathbf{K}_2 \mathbf{z}_2) \quad (26)$$

uniformly globally exponentially stable (UGES).

3) *Step 3:*

The parameter $\boldsymbol{\varphi}^*$ is however unknown and must be estimated as $\hat{\boldsymbol{\varphi}}$. The CLF is therefore expanded to

$$V_3 \triangleq \tilde{\boldsymbol{\varphi}}^\top \Gamma_\varphi^{-1} \tilde{\boldsymbol{\varphi}} + V_2, \quad (27)$$

where $\Gamma_\varphi > 0$ is the adaptation gain and $\tilde{\boldsymbol{\varphi}} \triangleq \boldsymbol{\varphi}^* - \hat{\boldsymbol{\varphi}}$. Hence, the control law in (23) is modified to

$$\boldsymbol{\tau} = \mathbf{M}\dot{\boldsymbol{\alpha}} + \mathbf{C}\boldsymbol{\nu} - \mathbf{g} - \Phi \hat{\boldsymbol{\varphi}} - \mathbf{z}_1 - \mathbf{K}_2 \mathbf{z}_2 \quad (28)$$

such that it uses the estimated parameter $\hat{\boldsymbol{\varphi}}$ instead of the real parameter, which changes the derivative of (21) to

$$\dot{V}_2 = -\mathbf{z}_1^\top \mathbf{K}_1 \mathbf{z}_1 - \mathbf{z}_2^\top \mathbf{K}_2 \mathbf{z}_2 + \tilde{\boldsymbol{\varphi}}^\top \Phi^\top \mathbf{z}_2. \quad (29)$$

The derivative of (27) then becomes

$$\dot{V}_3 = -\mathbf{z}_1^\top \mathbf{K}_1 \mathbf{z}_1 - \mathbf{z}_2^\top \mathbf{K}_2 \mathbf{z}_2 + \tilde{\boldsymbol{\varphi}}^\top (\Phi^\top \mathbf{z}_2 - \Gamma_\varphi^{-1} \dot{\tilde{\boldsymbol{\varphi}}}), \quad (30)$$

where the assumption that $\boldsymbol{\varphi}^*$ is constant or slowly varying relative to the vessel dynamics, has been applied. Hence, the adaptation law

$$\dot{\hat{\boldsymbol{\varphi}}} = \Gamma_\varphi \Phi^\top \mathbf{z}_2 \quad (31)$$

is chosen, which results in

$$\dot{V}_3 = -\mathbf{z}_1^\top \mathbf{K}_1 \mathbf{z}_1 - \mathbf{z}_2^\top \mathbf{K}_2 \mathbf{z}_2 \leq 0 \quad \forall \mathbf{z}_1, \mathbf{z}_2.$$

4) *Stability Analysis:*

The total closed-loop dynamics become

$$\dot{\mathbf{z}}_1 = \mathbf{S}^\top \mathbf{z}_1 - \mathbf{K}_1 \mathbf{z}_1 + \mathbf{z}_2 \quad (32)$$

$$\dot{\mathbf{z}}_2 = -\mathbf{M}^{-1}(\mathbf{z}_1 + \mathbf{K}_2 \mathbf{z}_2 - \Phi \tilde{\boldsymbol{\varphi}}) \quad (33)$$

$$\dot{\tilde{\boldsymbol{\varphi}}} = -\Gamma_\varphi \Phi^\top \mathbf{z}_2. \quad (34)$$

It can hence be concluded that the origin of the error system $(\mathbf{z}_1, \mathbf{z}_2, \tilde{\boldsymbol{\varphi}})$ is uniformly globally asymptotically stable (UGAS) by utilising Theorem A.6 from [12].

B. Concurrent Learning Backstepping

Concurrent learning is an adaptation concept based on the intuition that if the recorded data is sufficiently rich, i.e., there is a linear independence in the data, concurrent learning adaptation can be used to estimate true values without the need for persistency of excitation in the instantaneous data. However, Condition 1 from [6] needs to be fulfilled:

Condition 1: The recorded data has as many linearly independent elements as the dimension of the regressor matrix $\Omega(\mathbf{x}(t)) \in \mathbb{R}^{l \times m}$. That is if $\mathbf{Z} = [\Omega(\mathbf{x}(t_1))^\top, \Omega(\mathbf{x}(t_2))^\top, \dots, \Omega(\mathbf{x}(t_p))^\top]^\top$, then $\text{rank}(\mathbf{Z}) = m$.

1) *Composite Adaptation Law:*

If Condition 1 is satisfied for the regressor matrix Φ , the adaptation law (31) can be changed to

$$\dot{\hat{\boldsymbol{\varphi}}} = \Gamma_\varphi \left(\Phi^\top \mathbf{z}_2 + \sum_{j=1}^p \Phi_j^\top \boldsymbol{\epsilon}_j \right), \quad (35)$$

where $j \in \{1, 2, \dots, p\}$ denotes the index of a recorded data point $\mathbf{x}_j = [\boldsymbol{\eta}_j^\top, \boldsymbol{\nu}_j^\top]^\top$ and Φ_j is the regressor matrix evaluated at point \mathbf{x}_j , while $\boldsymbol{\epsilon}$ is an approximation error defined as

$$\boldsymbol{\epsilon} \triangleq \mathbf{y} - \hat{\mathbf{y}} \quad (36)$$

where

$$\begin{aligned}\mathbf{y} &= \Phi \boldsymbol{\varphi}^* \\ &= \mathbf{M}\dot{\boldsymbol{\nu}} - \boldsymbol{\tau} + \mathbf{C}(\boldsymbol{\nu})\boldsymbol{\nu} - \mathbf{g}(\boldsymbol{\nu})\end{aligned}\quad (37)$$

$$\hat{\mathbf{y}} = \Phi \hat{\boldsymbol{\varphi}}, \quad (38)$$

and it is assumed that the acceleration vector $\dot{\boldsymbol{\nu}}$ can be measured. Hence, (35) is a composite adaptation law since it both uses the control error \mathbf{z}_2 and the approximation error $\boldsymbol{\epsilon}$ to update the estimate of the uncertainties, see [15]. By combining the control law (28) and the new adaptation law (35), the derivative of (27) becomes

$$\begin{aligned}\dot{V}_3 &= -\mathbf{z}_1^\top \mathbf{K}_1 \mathbf{z}_1 - \mathbf{z}_2^\top \mathbf{K}_2 \mathbf{z}_2 - \tilde{\boldsymbol{\varphi}}^\top \sum_{j=1}^p \Phi_j^\top \boldsymbol{\epsilon}_j \\ &= -\mathbf{z}_1^\top \mathbf{K}_1 \mathbf{z}_1 - \mathbf{z}_2^\top \mathbf{K}_2 \mathbf{z}_2 - \tilde{\boldsymbol{\varphi}}^\top \sum_{j=1}^p \Phi_j^\top (\Phi_j \tilde{\boldsymbol{\varphi}}).\end{aligned}\quad (39)$$

Note that $\sum_{j=1}^p \Phi_j^\top \Phi_j > 0$ due to Condition 1. Hence, it can be shown that the origin of the error system $(\mathbf{z}_1, \mathbf{z}_2, \tilde{\boldsymbol{\varphi}})$ is UGES by utilising Theorem 4.10 from [16].

2) *Cascaded Adaptation Law:*

We can also change (35) to

$$\dot{\hat{\boldsymbol{\varphi}}} = \Gamma_\varphi \left(\Phi^\top \boldsymbol{\epsilon} + \sum_{j=1}^p \Phi_j^\top \boldsymbol{\epsilon}_j \right), \quad (40)$$

such that the adaptation dynamics are in cascade with the controller and only uses the approximation error to calculate the estimate of the model uncertainties. Hence, (40) is no longer a composite adaptation law since the control error \mathbf{z}_2 has been replaced by the approximation error $\boldsymbol{\epsilon}$.

In this case, it can be concluded that the origin of \mathbf{z}_1 and \mathbf{z}_2 is UGES when seeing $\tilde{\varphi}$ as an input with $\tilde{\varphi} = \mathbf{0}$. Consequently, it can be concluded by Lemma 4.6 from [16] that the subsystem (32) and (33) is input-to-state stable (ISS).

Using the CLF

$$V_4 \triangleq \tilde{\varphi}^\top \Gamma_\varphi^{-1} \tilde{\varphi}, \quad (41)$$

it can be shown that the origin of the adaptation error dynamics $\tilde{\varphi}$ becomes UGES when using (40).

The total closed-loop dynamics now become

$$\dot{\mathbf{z}}_1 = \mathbf{S}^\top \mathbf{z}_1 - \mathbf{K}_1 \mathbf{z}_1 + \mathbf{z}_2 \quad (42)$$

$$\dot{\mathbf{z}}_2 = -\mathbf{M}^{-1}(\mathbf{z}_1 + \mathbf{K}_2 \mathbf{z}_2 - \Phi \tilde{\varphi}) \quad (43)$$

$$\dot{\tilde{\varphi}} = -\Gamma_\varphi \left(\Phi^\top \epsilon + \sum_{j=1}^p \Phi_j^\top \epsilon_j \right). \quad (44)$$

Since the stability of the origin of the \mathbf{z}_1 and \mathbf{z}_2 subsystem in (42) and (43) is UGES for $\tilde{\varphi} = 0$, and utilising Theorem 2.1 from [17], it can be concluded that the origin of the total system $(\mathbf{z}_1, \mathbf{z}_2, \tilde{\varphi})$ is UGES.

3) Data Storage Algorithm:

From (40), the convergence rate is related to the summation of the stored data. The concurrent learning gives the option of choosing which data to store for this summation. An algorithm is therefore chosen such that the data stored is diverse, which ensures full rank of the matrix \mathbf{Z} from Condition 1.

The data window algorithm, described in Algorithm 1, works like a queue with a constant number of matrices, such that if a new measurement is sufficiently different from the previous one, then the new regression matrix is stored and the oldest regression matrix is rejected.

Algorithm 1 Pseudocode for the data window choosing algorithm

- 1: $end \leftarrow SM$ { % number of stored matrices in the queue }
 - 2: $[m, n] \leftarrow \text{size}(\Phi(\nu_0))$
 - 3: $\Phi_M \leftarrow \text{zeros}(SM, m, n)$ { % Initializing the storage matrix }
 - 4: $\Upsilon_M \leftarrow \text{zeros}(SM, m, 1)$ { % Initializing the error storage matrix }
 - 5: **for** $i = 1$ to $endTime$ **do**
 - 6: $\Phi_{temp} \leftarrow \Phi(\nu_i)$
 - 7: $\Phi_p \leftarrow \Phi_M[1]$
 - 8: **if** $\text{norm}(\Phi_{temp} - \Phi_p) < \delta$ **then**
 - 9: $\Phi_M[2 : end] \leftarrow \Phi_M[1 : end - 1]$
 - 10: $\Phi_M[1] \leftarrow \Phi_{temp}$ { % Queuing the regression matrices }
 - 11: $\Upsilon_M[2 : end] \leftarrow \Upsilon_M[1 : end - 1]$
 - 12: $\Upsilon_M[1] \leftarrow \mathbf{y}_i$ { % Queuing the y error vectors }
 - 13: $\mathcal{E} = \Upsilon_M - \Phi_M * \tilde{\varphi}_i$
 - 14: $\Sigma = \Phi_M * \mathcal{E}$ { % Multiplication like the sum in (40) }
 - 15: **end if**
 - 16: **end for**
-

X_{uuu}^*	-3.787	$X_{ u u}^*$	0.3545
$Y_{ v v}^*$	-2.776	$Y_{ r v}^*$	-0.805
Y_r^*	-7250	$Y_{ v r}^*$	-0.845
$Y_{ r r}^*$	-3.450	$N_{ v v}^*$	-0.2088
$N_{ r v}^*$	0.130	N_r^*	-1.900
$N_{ v r}^*$	0.080	$N_{ r r}^*$	-0.750

TABLE I: Model parameters

IV. SIMULATION RESULTS AND PERFORMANCE EVALUATION

This section starts with describing the vessel model, followed by the target motion, initial states and control parameters used in the simulations. Subsequently, performance metrics used to evaluate the the control performance are defined. Finally, the simulation results are presented and discussed.

A. Simulation Setup

1) Vessel Model Parameters:

The model-scale ship Cybership Enterprise I, with parameters from [11], will be used to test the performance of the adaptive controllers through numerical simulations in Matlab. Cybership Enterprise I is a 1:70 scale replica of a supply ship, with a length of $L = 1.105$ (m). It is fully actuated with two Voith-Schneider propellers aft and one bow thruster.

The model parameters for the vessel are chosen as shown in Table I.

2) Target Motion, Initial States and Control Parameters:

For an elliptic target motion, the target pose $\eta_t(t)$ is derived from

$$\eta_t(t) = \left[x_t(t), y_t(t), \frac{\pi}{2} - \arctan \left(\frac{\dot{y}_t(t)}{\dot{x}_t(t)} \right) \right]^\top, \quad (45)$$

where

$$x_t(t) = 5 + \sin \left(\frac{\pi}{180} \theta(t) \right) \quad (46)$$

$$y_t(t) = 0.5 + 1.5 \cos \left(\frac{\pi}{180} \theta(t) \right), \quad (47)$$

and

$$\dot{\theta}(t) = \frac{v_t}{\frac{\pi}{180} \sqrt{\left(\cos \left(\frac{\pi}{180} \theta(t) \right) \right)^2 + \left(1.5 \sin \left(\frac{\pi}{180} \theta(t) \right) \right)^2}}. \quad (48)$$

The reference target has a constant speed $v_t = 0.15$ (m/s). For the full-scale vessel, this corresponds to 1.275 m/s using the Bis scale [12]. By taking the time derivative, $\dot{\eta}_t(t)$ and $\ddot{\eta}_t(t)$ can be found.

The initial condition of the target trajectory is chosen to be $\theta(0) = 0$ and $\eta_t(0) = [5$ (m), 2 (m), 0 (rad)][⊤].

The initial vessel states are chosen to be $\eta(0) = [5.5$ (m), 2.5 (m), $\frac{1}{4}\pi$ (rad)][⊤] and $\nu(0) = [0$ (m/s), 0 (m/s), 0 (rad/s)][⊤]. The control and adaptation gains in Table II are obtained after iterative tuning, since it is assumed that there are no magnitude or rate saturation constraints for the control input τ . It should be noted that all of the adaptive controllers use the same gain matrices. The data window was chosen

to have a size of 10 such that it both uses recorded and instantaneous data and at the same time does not require a large amount of computational power.

\mathbf{K}_1	$diag([0.4, 0.4, 0.1])$
\mathbf{K}_2	$diag([5, 8, 6])$
Γ_φ	$diag([8, 8, 8, 8, 4, 8, 8, 8, 8, 4, 8, 8])$

TABLE II: Control and adaptation gains

The initial values for the estimated model parameters are $\hat{\varphi}(0) = \mathbf{0}_{12 \times 1}$.

3) Performance Metrics:

To evaluate and compare the performance of the control algorithms, performance metrics must be defined and used. These include the integral of the absolute error (IAE) for a chosen error metric. For this, we will use the norm of the pose error e , which can be calculated by

$$e(t) = \sqrt{\tilde{\eta}(t)^\top \tilde{\eta}(t)}. \quad (49)$$

The IAE is then calculated as

$$IAE(t) = \int_0^t |e(\sigma)| d\sigma, \quad (50)$$

which simply describes the temporal evolution of the absolute value of the error without adding any weight to the error.

Finally, we will use combination of the integral of the absolute error multiplied by the energy consumption (IAEW), which was proposed in [5] and evaluate the property of how smooth the controller is by how fast τ is changing, thus including $\dot{\tau}$. If the control input is smooth, it is more realistic that “wear and tear” of the actuator is reduced. Multiplying all these effects together gives the metric integral of the absolute error with work, wear and tear (IAEW-WT), which was proposed in [9] and is defined as

$$IAEW-WT(t) = \int_0^t |e(\sigma)| d\sigma \int_0^t P(\sigma) d\sigma \int_0^t \|\dot{\tau}(\sigma)\| d\sigma, \quad (51)$$

where

$$P(t) = |\nu(t)^\top \tau(t)| \quad (52)$$

represents the mechanical power. We compute the change of control input as

$$\dot{\tau}(t) = \frac{\tau(t) - \tau(t-h)}{h}, \quad (53)$$

where h is the sample time.

B. Simulation Results

In the following plots, AB refers to the adaptive backstepping controller, CL-CO refers to the concurrent learning backstepping controller with the composite adaptation law, while CL-CA refers to the concurrent learning backstepping controller with the cascaded adaptation law.

In Fig. 1, the vessel and target pose outlines are plotted to show the transient convergence behavior. Here, the blue

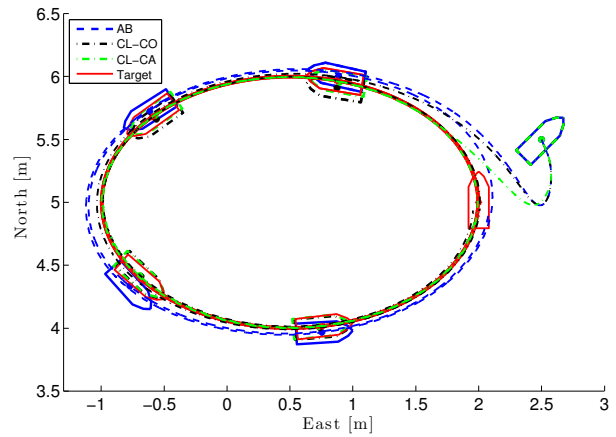


Fig. 1: The vessel tracking the target which is moving along an elliptical path

outline represents the AB-controlled vessel, the dash-dotted black outline represents the CL-CO-controlled vessel, the dash-dotted green outline represents the CL-CA-controlled vessel, while the red solid outline represents the target. It should be noted that the outlined vessels have been scaled down for increased readability of the figure. Here, it can easily be seen that CL-CA controller has a better control performance than the two others.

Fig. 2 illustrates the normed pose error e scaled by the vessel length L , showing that all controllers are able to converge to a neighbourhood of the target, which is due to the fact that the assumption $\dot{\varphi}^* = \mathbf{0}$ is not satisfied. It is worth noting that the introduction of cascaded concurrent learning leads to faster convergence despite identical gain matrices \mathbf{K}_1 , \mathbf{K}_2 and Γ_φ for all the controllers.

The phase-portrait relation between the normed error variables \mathbf{z}_1 and \mathbf{z}_2 is shown in Fig. 2b. Here, we can see that the controller with cascaded concurrent learning is able to reduce the initial increase in \mathbf{z}_1 marginally faster than the standard adaptive backstepping controller and the composite concurrent learning, and achieve a sharper trajectory toward the origin of the \mathbf{z} -dynamics. In Fig. 3a, the normed control input of the controllers is shown. In addition, the feedforward, feedback and adaptive parts of the normed control input are plotted separately in Fig 3b, 3c and 3d, where

$$\tau_{FF} = \mathbf{M}\dot{\alpha} + \mathbf{C}(\nu)\nu - \mathbf{g}(\nu) \quad (54)$$

$$\tau_{FB} = -\mathbf{z}_1 - \mathbf{K}_2\mathbf{z}_2 \quad (55)$$

$$\tau_{AD} = -\Phi(\nu)\hat{\varphi}. \quad (56)$$

Note that Fig. 3a-d only show the first 100 seconds of the simulation. It is hard to distinguish the normed control input of the controllers in Fig. 3a. However, by splitting the signal into its components (54)-(56), it can be seen that the adaptive backstepping controller uses most energy in the feedback part of the control law, while the concurrent learning backstepping controllers use most energy in the feedforward part. In addition, Fig. 3d shows that the CL-CA controller also uses significant energy in the adaptive

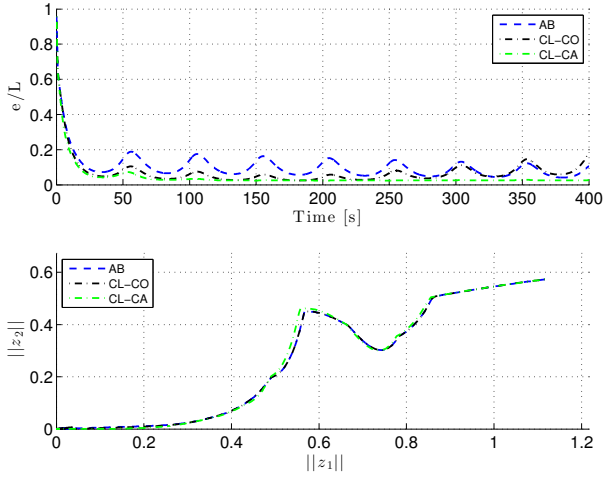


Fig. 2: The normed pose error scaled by the vessel length (top) and the phase portrait of the normed z -dynamics (bottom)

part of the control input.

In Fig. 4, the normed error between the real and the estimated damping forces is shown, where

$$\omega/defeqg(\nu) + \Phi(\nu)\hat{\varphi} + D(\nu)\nu. \quad (57)$$

Here, the CL-CA controller has the fastest convergence rate. However, the CL-CO controller has a good convergence rate in the beginning, but after some time it starts to diverge from zero, which affects the pose error, see also Fig. 2a. We have yet to find out why this happens.

Fig. 5 display the curves of the performance metrics IAE and IAEW-WT for the normed pose error. The figure indicates that the cascaded concurrent learning concept improves the tracking performance. In particular, Fig. 5a shows that the CL-CA controller has the fastest transient response since it quickly establishes the smallest IAE value. In addition, Fig. 5b shows that this controller has a significantly smaller value for the combined control accuracy, energy use and actuator wear and tear, thus achieving the best overall performance for this scenario.

V. CONCLUSION

This paper uses the adaptive backstepping controller as a benchmark controller to evaluate the control performance of two different combinations of the concurrent learning concept with the traditional backstepping controller: A concurrent learning backstepping controller with a composite adaptation law and a concurrent learning backstepping controller with a cascaded adaptation law. Simulations are conducted with a nonlinear 3 degrees-of-freedom model of a marine surface vessel, showing the considered controllers have a good tracking performance and the ability to adapt for model uncertainties. The simulations also show that the concurrent learning backstepping controller with cascaded adaptation has the best control performance and is better at handling uncertainties than the other two controllers.

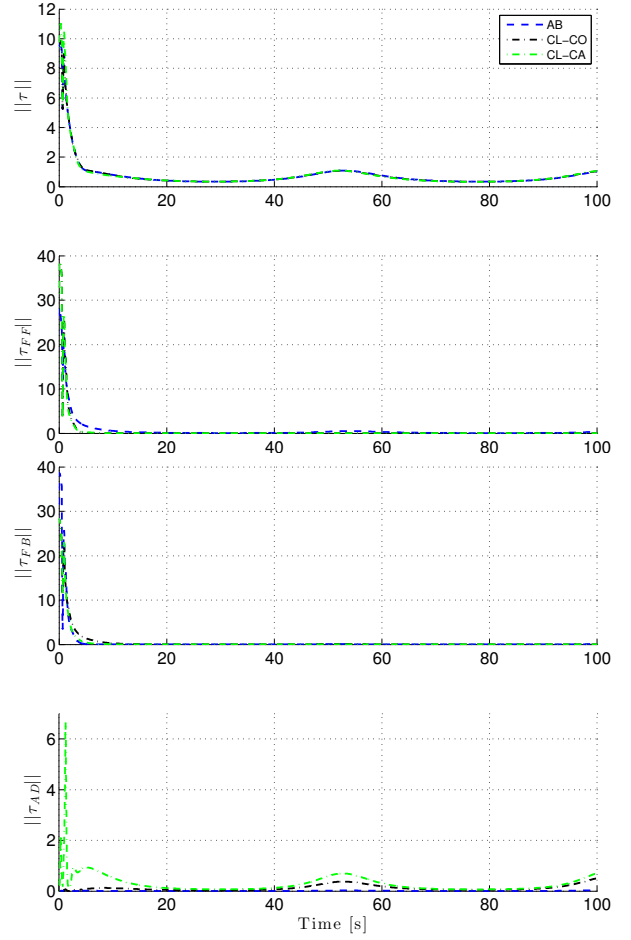


Fig. 3: The normed control input (top), the feedforward part of the normed control input (upper middle), the feedback part of the normed control input (lower middle) and the adaptive part of the normed control input (bottom)

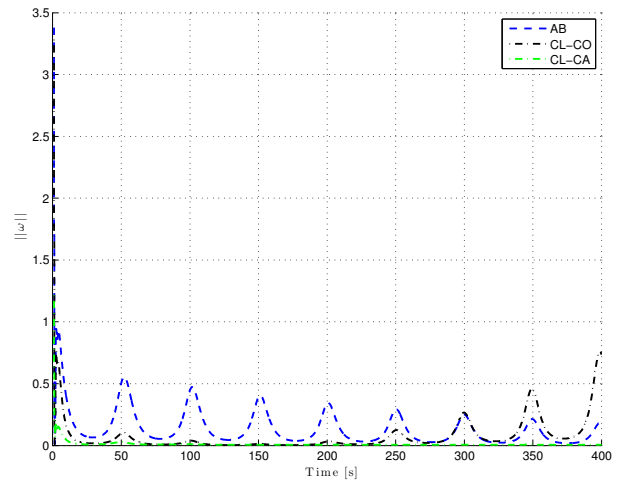


Fig. 4: The normed error between the real and the estimated damping forces

Future work includes improving the concurrent learning

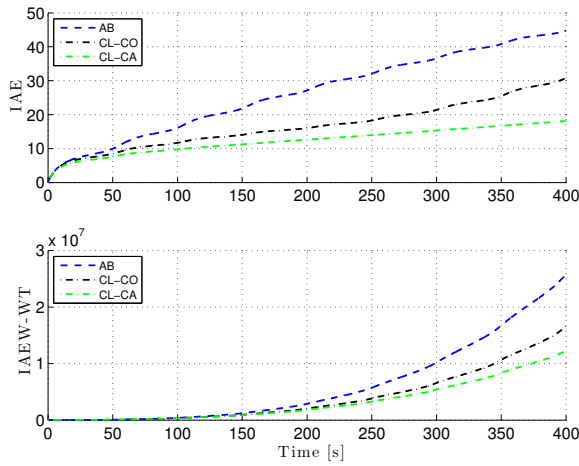


Fig. 5: The IAE and IAEW-WT performance metrics

adaptation algorithm such that it does not require acceleration measurements. Also, it is desirable to investigate why the composite concurrent learning starts to go into a limit cycle and try other concurrent learning adaptation algorithms which might further improve performance. Finally, it is desirable to verify the results experimentally by implementing and testing the controllers on a model-scale vessel.

ACKNOWLEDGEMENT

This work was supported by the Research Council of Norway through the Centres of Excellence funding scheme, project number 223254.

REFERENCES

- [1] E. Lavretsky and K. A. Wise, *Robust and Adaptive Control with Aerospace Applications*. Springer, 2012.
- [2] N. Hovakimyan and C. Cao, \mathcal{L}_1 Adaptive Control Theory: Guaranteed Robustness with Fast Adaptation. SIAM, 2010.

- [3] A. Astolfi, D. Karagiannis, and R. Ortega, *Nonlinear and Adaptive Control with Applications*. Springer, 2008.
- [4] T. Yucelen and E. Johnson, “Command governor-based adaptive control,” in *Proceedings of AIAA Guidance, Navigation, and Control Conference, Minneapolis, USA*, 2012.
- [5] M. E. N. Sørensen and M. Breivik, “Comparing nonlinear adaptive motion controllers for marine surface vessels,” in *Proceedings of the 10th IFAC Conference on Manoeuvring and Control of Marine Craft, Copenhagen, Denmark*, 2015.
- [6] G. Chowdhary and E. Johnson, “Concurrent learning for convergence in adaptive control without persistency of excitation,” in *Proceedings of the 49th IEEE Conference on Decision and Control, Atlanta, USA*, 2010.
- [7] G. Chowdhary, M. Culterz, N. K. Üre, and J. P. How, “Experimental results of concurrent learning adaptive controllers,” in *Proceedings of the AIAA Guidance, Navigation, and Control Conference, Minneapolis, USA*, 2012.
- [8] B. Reish and G. Chowdhary, “Concurrent learning adaptive control for systems with unknown sign of control effectiveness,” in *Proceedings of the 53rd IEEE Conference on Decision and Control, Los Angeles, USA*, 2014.
- [9] E. S. Bjørne, *Nonlinear Adaptive Motion Control and Model-Error Analysis for Ships*. MSc thesis. Dept. of Engineering Cybernetics, Norwegian University of Science and Technology, Trondheim, Norway, 2016.
- [10] M. Krstic, I. Kanellakopoulos, and P. V. Kokotovic, *Nonlinear and Adaptive Control Design*. Wiley, 1995.
- [11] F. Sandved, *Remote Control and Automatic Path-following for C/S Enterprise I and ROV Neptunus*. MSc thesis. Dept. of Marine Technology, Norwegian University of Science and Technology, Trondheim, Norway, 2015.
- [12] T. I. Fossen, *Handbook of Marine Craft Hydrodynamics and Motion Control*. Wiley, 2011.
- [13] R. Skjetne, Ø. N. Smogeli, and T. I. Fossen, “Nonlinear Ship Manoeuvring Model: Identification and Adaptive Control with Experiments for a Model Ship,” *Modeling, Identification and Control*, vol. 25, no. 1, pp. 3–27, 2004.
- [14] T. I. Fossen and J. P. Strand, “Tutorial on Nonlinear Backstepping: Applications to Ship Control,” *Modeling, Identification and Control*, vol. 20, no. 2, pp. 83–135, 1999.
- [15] J.-J. E. Slotine and W. Li, *Applied Nonlinear Control*. Prentice Hall, 1991.
- [16] H. K. Khalil, *Nonlinear Systems*. Prentice Hall, 2002.
- [17] F. Lamnabhi-Lagarrigue, E. Panteley, E. Lefeber, and A. Loria, *Advanced Topics in Control Systems Theory: Lecture Notes from FAP 2004*. Springer, 2005.